Modeling collagen fibril degradation as a function of matrix microarchitecture: Supplementary Information

Bhanjan Debnath[1], Badri Narayanan Narasimhan[2], Stephanie I Fraley[2], and Padmini Rangamani[1,3]

[1]*Department of Mechanical and Aerospace Engineering, University of California San Diego, CA 92093, USA*

[2]*Department of Bioengineering, University of California San Diego, CA 92093, USA*

[3]*Department of Pharmacology, School of Medicine, University of California San Diego, CA 92093, USA*

Supplementary Information (SI)

SI1 Reaction scheme:

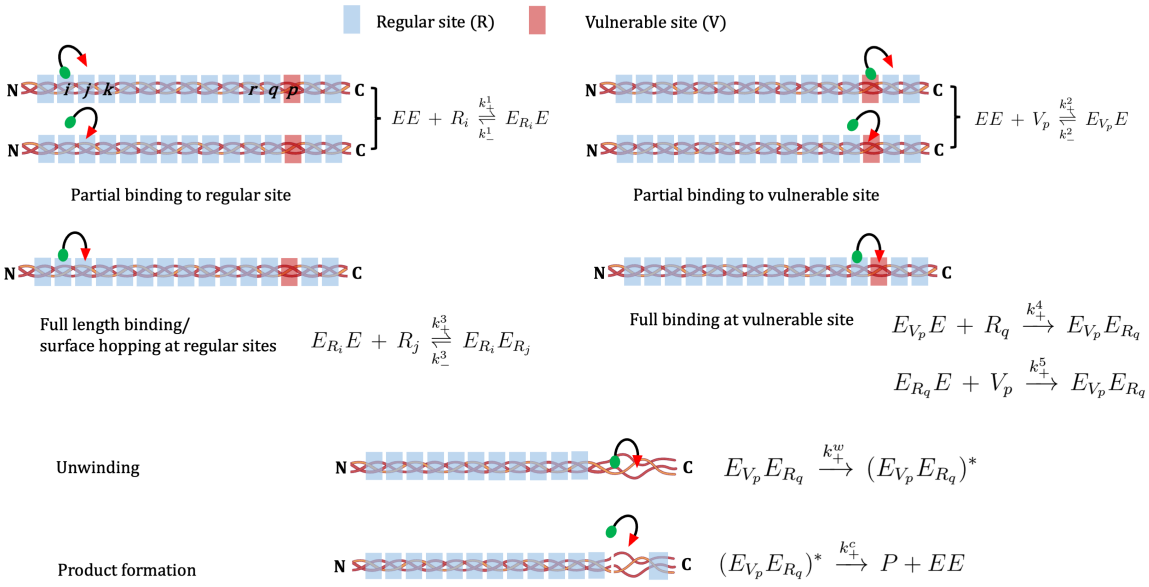

Figure S1: Schematic of the enzyme kinetics.

SI2 Adsorption kinetics and Φ_{ad}:

For reversible partial binding (represented by eqn (3) of the main text), we implemented the protein adsorption-desorption kinetics [1, 2]. The rate of adsorption is proportional to the available surface function $\Phi_{ad} = 1 - (\theta/\theta_{max})$. This available surface function is related to the steric hindrance during adsorption [1, 3, 2], where θ and θ_{max} are the surface coverage fraction and its maximum saturated value, respectively. If the number of total enzymes is very small compared to the number of available sites, $\Phi_{ad}(\theta) \to 1$ in the limit of very low surface coverage. If the limit of low surface coverage does not hold true, some descriptions related to $\Phi_{ad}(\theta)$ are provided in earlier work [4, 5, 3]. In our work, the limit $N^s \gg N_{EE}(t = 0)$ holds true for low concentration of enzyme, where N^s and N_{EE} are total number of sites exposed at the surface and number of enzymes, respectively. Thus we set $\Phi_{ad} = 1$.

SI3 Correction factor ϕ in the intrinsic rates of full-length binding kinetics:

In our model, we treated the forward rates of eqns (4)–(5) of the main text as pseudo first-order kinetics multiplied with a correction factor ϕ. The functional form of ϕ increases with the number (n_a) of available lattice sites per enzyme at partially bound state. The value of ϕ is zero if there is no site available, $\phi = 1$ when only one lattice site is available ($n_a = 1$), and ϕ must saturate around $(\pi\,(d_E)^2)/(d_m\,d_{\mathrm{TC}})$ which is equivalent to the number of lattice sites inside the searching radius d_E (see Fig. 1b,c of the main text). We proposed a phenomenological function for ϕ as

$$\phi \approx \frac{\pi\,(d_E)^2}{d_m\,d_{\mathrm{TC}}}\,\frac{n_a}{c_1 + n_a}, \tag{S1}$$

where $n_a = N^s/(N^s_{E_RE} + N^s_{E_VE})$, N^s is the number of available sites on the fibril surface, $N^s_{E_RE}$ and $N^s_{E_VE}$ are the number of enzymes partially bound to one regular site and one vulnerable site, respectively. Here $c_1 = 25$ is a dimensionless constant which is

obtained by setting $\phi(n_a = 1) = 1$ for $d_E = 10$ nm, $d_{\mathrm{TC}} = 1.5$ nm and $d_m = 8$ nm.

SI4 System of ODEs:

The system of ODEs representing the reaction scheme eqns (3)–(7) of the main text is the following

$$\begin{aligned}
\frac{\mathrm{d}N_{EE}}{\mathrm{d}t} &= -\,k_+^1\,N_{EE}\,\Phi_{ad}(\theta) + k_-^1\,N^s_{E_RE} - k_+^2\,N_{EE}\,\Phi_{ad}(\theta) + k_-^2\,N^s_{E_VE} \\
&\quad + k_+^c\,N^s_{(E_VE_R)^*} && \text{(S2)}\\
\frac{\mathrm{d}N^s_R}{\mathrm{d}t} &= -\,k_+^1\,N_{EE}\,\Phi_{ad}(\theta) + k_-^1\,N^s_{E_RE} - k_+^3\,N^s_{E_RE}\,\phi + k_-^3\,N^s_{E_RE_R} \\
&\quad - k_+^4\,N^s_{E_VE}\,\phi - \Re && \text{(S3)}\\
\frac{\mathrm{d}N^s_V}{\mathrm{d}t} &= -\,k_+^2\,N_{EE}\,\Phi_{ad}(\theta) + k_-^2\,N^s_{E_VE} - k_+^5\,N^s_{E_RE} && \text{(S4)}\\
\frac{\mathrm{d}N^s_{E_RE}}{\mathrm{d}t} &= k_+^1\,N_{EE}\,\Phi_{ad}(\theta) - k_-^1\,N^s_{E_RE} - k_+^3\,N^s_{E_RE}\,\phi + k_-^3\,N^s_{E_RE_R} \\
&\quad - k_+^5\,N^s_{E_RE} && \text{(S5)}\\
\frac{\mathrm{d}N^s_{E_VE}}{\mathrm{d}t} &= k_+^2\,N_{EE}\,\Phi_{ad}(\theta) - k_-^2\,N^s_{E_VE} - k_+^4\,N^s_{E_VE}\,\phi && \text{(S6)}\\
\frac{\mathrm{d}N^s_{E_RE_R}}{\mathrm{d}t} &= k_+^3\,N^s_{E_RE}\,\phi - k_-^3\,N^s_{E_RE_R} && \text{(S7)}\\
\frac{\mathrm{d}N^s_{E_VE_R}}{\mathrm{d}t} &= k_+^4\,N^s_{E_VE}\,\phi + k_+^5\,N^s_{E_RE} - k_+^w\,N^s_{E_VE_R} && \text{(S8)}\\
\frac{\mathrm{d}N^s_{(E_VE_R)^*}}{\mathrm{d}t} &= k_+^w\,N^s_{E_VE_R} - k_+^c\,N^s_{(E_VE_R)^*} && \text{(S9)}\\
\frac{\mathrm{d}N_P}{\mathrm{d}t} &= k_+^c\,N^s_{(E_VE_R)^*} + \frac{1}{2}\Re\,, && \text{(S10)}
\end{aligned}$$

where N_{EE}, N^s_R, N^s_V, $N^s_{E_RE}$, $N^s_{E_VE}$, $N^s_{E_RE_R}$, $N^s_{E_VE_R}$, $N^s_{(E_VE_R)^*}$, N_P are numbers of free enzymes, regular sites, vulnerable sites, enzymes partially bound to one regular site, enzymes partially bound to one vulnerable site, enzymes fully bound to two regular sites, enzymes fully bound to one regular and one vulnerable site, enzymes fully bound to one regular and one vulnerable site (unwound state), and product sites, respectively. Here k_+^1, k_-^1, k_+^2, k_-^2, k_+^3, k_-^3, k_+^4, k_+^5, k_+^w, and k_+^c are the reaction rate constants having

dimension $[\text{time}]^{-1}$; Φ_{ad} and ϕ are available surface function and correction factor related to adsorption kinetics and full-length binding/hopping kinetics, respectively. We included another term $\Re$ in the series of ODEs (eqns (S2)-(S10)) in an *ad hoc* manner, which is related to force-assisted removal of regular sites. We discussed about $\Re$ in the main text and in the next section. The balances for the total number of enzymes and total number of sites are the following.

Balance for total number of enzymes:

$$\begin{aligned}
&\frac{\mathrm{d}N_{EE}}{\mathrm{d}t} + \frac{\mathrm{d}N^s_{E_RE}}{\mathrm{d}t} + \frac{\mathrm{d}N^s_{E_VE}}{\mathrm{d}t} + \frac{\mathrm{d}N^s_{E_RE_R}}{\mathrm{d}t} + \frac{\mathrm{d}N^s_{E_VE_R}}{\mathrm{d}t} + \frac{\mathrm{d}N^s_{(E_VE_R)^*}}{\mathrm{d}t} \\
&= \Big[- k^1_+ N_{EE}\,\Phi_{ad}(\theta) + k^1_- N^s_{E_RE} - k^2_+ N_{EE}\,\Phi_{ad}(\theta) + k^2_- N^s_{E_VE} + k^c_+ N^s_{(E_VE_R)^*} \Big] \\
&+ \Big[k^1_+ N_{EE}\,\Phi_{ad}(\theta) - k^1_- N^s_{E_RE} - k^3_+ N^s_{E_RE}\,\phi + k^3_- N^s_{E_RE_R} - k^5_+ N^s_{E_RE} \Big] \\
&+ \Big[k^2_+ N_{EE}\,\Phi_{ad}(\theta) - k^2_- N^s_{E_VE} - k^4_+ N^s_{E_VE}\,\phi \Big] + \Big[k^3_+ N^s_{E_RE}\,\phi - k^3_- N^s_{E_RE_R} \Big] \\
&+ \Big[k^4_+ N^s_{E_VE}\,\phi + k^5_+ N^s_{E_RE} - k^w_+ N^s_{E_VE_R} \Big] + \Big[k^w_+ N^s_{E_VE_R} - k^c_+ N^s_{(E_VE_R)^*} \Big] \\
&= 0
\end{aligned} \tag{S11}$$

Balance for total number of lattice sites:

$$\begin{aligned}
&\frac{\mathrm{d}N^s_R}{\mathrm{d}t} + \frac{\mathrm{d}N^s_V}{\mathrm{d}t} + \frac{\mathrm{d}N^s_{E_RE}}{\mathrm{d}t} + \frac{\mathrm{d}N^s_{E_VE}}{\mathrm{d}t} + 2\,\frac{\mathrm{d}N^s_{E_RE_R}}{\mathrm{d}t} + 2\,\frac{\mathrm{d}N^s_{E_VE_R}}{\mathrm{d}t} + 2\frac{\mathrm{d}N^s_{(E_VE_R)^*}}{\mathrm{d}t} + 2\frac{\mathrm{d}N_p}{\mathrm{d}t} \\
&= \Big[- k^1_+ N_{EE}\,\Phi_{ad}(\theta) + k^1_- N^s_{E_RE} - k^3_+ N^s_{E_RE}\,\phi + k^3_- N^s_{E_RE_R} - k^4_+ N^s_{E_VE}\,\phi - \Re \Big] \\
&+ \Big[- k^2_+ N_{EE}\,\Phi_{ad}(\theta) + k^2_- N^s_{E_VE} - k^5_+ N^s_{E_RE} \Big] \\
&+ \Big[k^1_+ N_{EE}\,\Phi_{ad}(\theta) - k^1_- N^s_{E_RE} - k^3_+ N^s_{E_RE}\,\phi + k^3_- N^s_{E_RE_R} - k^5_+ N^s_{E_RE} \Big] \\
&+ \Big[k^2_+ N_{EE}\,\Phi_{ad}(\theta) - k^2_- N^s_{E_VE} - k^4_+ N^s_{E_VE}\,\phi \Big] \\
&+ 2\Big[k^3_+ N^s_{E_RE}\,\phi - k^3_- N^s_{E_RE_R} \Big] + 2\Big[k^4_+ N^s_{E_VE}\,\phi + k^5_+ N^s_{E_RE} - k^w_+ N^s_{E_VE_R} \Big] \\
&+ 2\Big[k^w_+ N^s_{E_VE_R} - k^c_+ N^s_{(E_VE_R)^*} \Big] + 2\Big[k^c_+ N^s_{(E_VE_R)^*} + \frac{1}{2}\Re \Big] \\
&= 0
\end{aligned} \tag{S12}$$

SI5 Force-assisted removal and description related to $\Re$:

We assumed that the energy barrier for temporary winding-unwinding of a lattice site due to thermal fluctuations is symmetric in absence of enzymes. Both the rates to cross the energy barrier from either side are proportional to $\exp\left(-E_m/(k_BT)\right)$ resulting in zero net rate, where E_m is the energy required to cross the barrier, k_B is the Boltzmann constant, and T is the temperature. Due to a force F emerging from enzyme-induced unwinding [6], the energy barrier for other regular sites can become asymmetric. The energy required for the transition towards unwinding is reduced to $(E_m - \lambda_m F)$, and for the other side, it is increased to $(E_m + \lambda_m F)$. Here λ_m is the extent of dissociation in unwound state which is chosen as ~ 3.6 Å [7]. Thus the net rate of flow over the energy barrier towards unwinding according to the theory of reaction rates is [8, 9]

$$k_R = \frac{k_BT}{h}\left[\exp\left(\frac{-(E_m - \lambda_m F)}{k_BT}\right) - \exp\left(\frac{-(E_m + \lambda_m F)}{k_BT}\right)\right], \tag{S13}$$

where h is Planck constant. For $F = 0$, the form (S13) yields to zero. Here the value of E_m is chosen as $E_m = n_{res}\,\Delta G/N_A$, where $\Delta G = 1.9$ kJ/mole per amino acid residue, N_A is Avogadro number, and $n_{res} = 28$ is the number of amino acid residues corresponding to one lattice site [7]. Thus the rate of force assisted removal of exposed regular sites is

$$\Re = k_R\, N_R^s, \tag{S14}$$

which is added in an *ad hoc* manner in the system of ODEs (eqn (S2)-(S10)). We derive the force F in a heuristic manner.

The force corresponding to the local stress generated during enzyme-induced unwinding at one lattice (vulnerable) site is equivalent to the force necessary to generate a new surface via slippage of the chain on the surface [10, 11, 12], i.e.

$$f \sim \gamma\, v_s\, \tau_c, \tag{S15}$$

where $\gamma \sim \frac{k_B T}{d_m d_{\mathrm{TC}}}$ is the surface energy per unit area [13, 14], $v_s \sim d_m\, k_+^c$ is the approximate velocity of slippage, and τ_c is a characteristic time. This characteristic time can be equivalent to the characteristic time of reptation of a polymer chain. The velocity of slippage v_s is approximately the multiplication of the length of the lattice site d_m to the frequency a chain experiences slippage events after cleavage i.e. k_+^c. Note that the form for f in eqn (S15) is due to one unwound vulnerable site in presence of one enzyme. Due to multiple unwound vulnerable sites (in presence of enzymes), the total average force can be proportional to the rate at which enzymatic unwinding happens, i.e., $2\, k_+^w\, N^s_{E_V E_R}$ (see eqn (6) of the main text). Thus the average force per remaining lattice sites can be

$$F \sim \frac{1}{N^s} \left(\gamma\, d_m\, k_+^c\, \tau_c\right) \left(2\, k_+^w\, N^s_{E_V E_R}\right) \tau_e, \tag{S16}$$

where τ_e is an average time required to form disentangled chains during detachment from the surface. When a fibril loses its lattice sites in degradation, dangling and entangled chains of the cleaved tropocollagen units (weakly attached to the fibril surface) appear continuously. In phenomenological manner and following the work of [15], we propose $\tau_e = \tau_r^0 + \tau_c \left(\exp(\nu) - 1\right)$ [10, 12], where ν is the number of lattice sites lost in form of disentangled chains during degradation. When ν is zero, i.e. in absence of degradation, $\tau_e = \tau_r^0$ can be treated as average relaxation time of a fibril. The value of τ_r^0 is 7 s [16, 17]. We treated τ_c as a material parameter and obtained its value as 1.4 s using the experimental data of single fibril degradation under zero loading condition (Flynn et al. [18]) (see section SI10 and Fig. S2a).

SI6 Reaction rate constants and other parameters:

We provided the values of rate constants and other parameters in table S1. Using the relation of protein adsorption-desorption rate constants [3], we set k_+^1 and k_-^1 where $k_-^1 = k_+^1 \exp\left(-\Delta U_{ad}/(k_B T)\right)$. We assumed that all unbinding events happen with same probability (backwards reactions of eqns (3) and (4) of the main text), and the corresponding rate constants are equal, i.e. $k_-^1 = k_-^2 = k_-^3 = 5.65 \times 10^{-3}$ s^{-1} [19].

Using the value of k_{-}^{1} and for a chosen potential barrier difference of $\Delta U_{ad} \sim k_B T$, $k_{+}^{1} = k_{+}^{2} = 0.0154$ s^{-1}. In experiments, the velocity of the enzyme on the collagen surface reported was $\sim 4.5 \times 10^{-6}$ m/s [20]. Using this reported value of the velocity, we set the forward rate constants of eqns (4) and (5) of the main text related to full-length binding/hopping. The minimum distance an enzyme can traverse to find another lattice site for full-length binding or jump to change track is $d_{\rm TC} = 1.5$ nm, which sets $k_{+}^{3} = k_{+}^{4} = 3 \times 10^{3}$ s^{-1}. However, as the probability of the occurrence represented by the second part of eqn (5) of the main text is expected to be lower compared to the other hopping events, we set the value of k_{+}^{5} in an approximate manner based on the minimum distance between two neighboring vulnerable sites which is $D_{gap} = 67$ nm, and it sets $k_{+}^{5} = (k_{+}^{3}/(D_{gap}/d_{\rm TC}))$ s^{-1}. Using the transition state theory, we set the rate constant for enzyme-induced irreversible unwinding eqn 6 of the main text as $k_{+}^{w} = (k_B T/h) \exp(-2\, E_m/k_B T)$, where $E_m = n_{res}\, \Delta G/N_A$, and $(E_V E_R)^*$ corresponds to two lattice sites. For $\Delta G = 1.9$ kJ/mole per amino acid residue [7], $n_{res} = 28$ for one lattice site, $N_A = 6.023 \times 10^{23}$ and a chosen temperature $T = 310$ K, it yields to $k_{+}^{w} = 7.5 \times 10^{-6}$ s^{-1}. The value of k_{+}^{c} is different for different types of collagenase and collagen substrate [21, 22, 23, 24, 25]. To test the present model, we used two values: $k_{+}^{c} = 0.472$ s^{-1} (fibroblast collagenase and native collagen type I) [21] and $k_{+}^{c} = 0.583$ s^{-1} (class I clostridium histolyticum collagenases and rat type I) [23].

SI7 Initial conditions to solve the ODEs:

We used MATLAB ODE23 solver to solve the ODEs using the following initial conditions. The nine first order ODEs (eqn (S2)-(S10)) require nine following initial conditions: at time $t = 0$, number of enzymes surrounding a fibril N_e^0, $N_R^s = (N^s)^0 - (N_V^s)^0$, $N_V^s = (N_V^s)^0$, $N_{E_R E}^s = 0$, $N_{E_V E}^s = 0$, $N_{E_R E_R}^s = 0$, $N_{E_V E_R}^s = 0$, $N_{(E_V E_R)^*}^s = 0$, and $N_P = 0$. For a fibril of initial diameter $d_f(t = 0) = d_f^0$ and length $\ell_f(t = 0) = \ell_f^0$, we obtained $(N^s)^0$ and $(N_V^s)^0$ using eqns (2) and (1) of the main text, respectively.

Parameter	Value
d_{TC}	1.5 nm [26]
ℓ_{TC}	300 nm [26]
D-band gap (D_{gap})	67 nm [26]
d_E	10 nm [27]
d_m	8 nm [7]
n_{res}	28 [7]
c_1	25 (discussed in the main text)
ΔG	1.9 kJ/mole per amino acid residue [7]
λ_m	3.6 Å[7]
$k_+^1 = k_+^2$	0.0154 s^{-1} [3]
$k_-^1 = k_-^2 = k_-^3$	5.65×10^{-3} s^{-1} [19]
$k_+^3 = k_+^4$	3×10^3 s^{-1} [20]
k_+^5	$(k_+^3/(D_{gap}/d_{\mathrm{TC}}))$
k_+^w	7.5×10^{-6} s^{-1} [7]
k_+^c	0.583 s^{-1} [21] or, 0.472 s^{-1} [23]
τ_r^0	7 s [16]
τ_c	1.4 s (obtained using experiment [18])

Table S1: List of parameters and their values.

SI8 Fibril fraction estimation in simulation box from collagen concentration:

To set the fibril fraction ϕ_f (the ratio of the volume of all collagen fibrils to the volume of the simulation box) in our simulations, we followed a crude analytical way converting the collagen concentration to ϕ_f. An example is the following. We consider a collagen concentration $\sim$ 2.5 mg/mL [28]. Note that we performed *in vitro* experiments using the same collagen concentration. For this chosen concentration and using the molecular weight of tropocollagen $\sim$ 300 kDa [29], the number of tropocollagen units in the simulation box volume (which is 125 µm^3) is $\sim 0.63 \times 10^6$. The volume of one tropocollagen is $\frac{\pi}{4} (d_{\mathrm{TC}})^2 \, \ell_{\mathrm{TC}}$. Thus the total volume of all tropocollagen molecules in the simulation box volume is 334×10^{-3} µm^3.

These tropocollagen molecules arrange and generate fibrils in a solvent medium. Because of the gaps in between tropocollagen molecules in a fibril in hydrated condition (which is difficult to estimate in the present work), the total volume of all fibrils must be higher than the total volume of all tropocollagen molecules. To obtain a nearly correct estimate of the total volume of all fibrils, we assumed packing factor for cylindrical tropocollagen in loosely packed condition as 0.4 (note that the value of packing factor for spheres in loosely packed state is in the range $0.4 - 0.56$). Thus the nearly corrected volume of all fibrils is $(334 \times 10^{-3}$ µm$^3)/0.4$, and this volume yields to a fibril fraction $\phi_f \sim 0.006$ for the chosen collagen concentration 2.5 mg/mL .

The collagen percentage in different organs (such as, brain, liver, heart, kidney, lung and colon, etc.) varies in the range $0.1 - 6\%$ [30]. We performed simulations with different values of ϕ_f in the range $0.003 - 0.03$, which is $0.3 - 3\%$.

SI9 Experimental methods:

Chemicals:

High concentration, rat tail acid extracted type I collagen was procured from Corning (Corning, NY). PEG (8000 Da) was ordered in powder form from Sigma-Aldrich (St

Louis, MO) and reconstituted in PBS (Life Technologies, Carlsbad, CA) immediately before usage with a final concentration of 100 mg/mL, and 1× reconstitution buffer was composed of sodium bicarbonate, HEPES free acid, and nanopure water.

Preparation of collagen gels with different microstructures:

First, PEG of required amounts to make a 2 or 8 mg/mL final concentration (denoted as P2 or P8) was added to the DMEM. This is followed by addition of the reconstitution buffer and mixing. Thereafter, the collagen stock was added to the mixture to produce a final concentration of 2.5 mg/mL. Finally, pH of the final mixture was adjusted using 1 N NaOH, followed by incubation ($\sim$ 45 minutes) at 37°C. Following polymerization, PEG was washed out of the gels by rinsing with the DMEM (3× for 5 minutes each). For collagenase treatment, gels were incubated with bacterial collagenase of 2.5 µg/mL for about 45 minutes. (We added 50 microliters of 10 microgram per mL of collagenase on top of the gels which yields final concentration of collagen to be 2.5 µg/mL.)

Fast green staining and imaging of collagen gels:

The prepared collagen gels were fixed with 4% paraformaldehyde for 30 mins. After that, the gels were washed thoroughly at least 3 times by subjecting them to shaking and replacing with PBS for 10 min. The gels were then incubated with 100 µg/mL of fast green dye in PBS (Fast green FCF, Thermo Fischer, USA) and were subjected to shaking overnight. The gels were washed with PBS at least 3 times in an orbital shaker for a duration of 30 minutes each time. The stained gels were then imaged using a confocal fluorescence microscope (Leica, SP8) with 40x water immersion objective. Fast green was excited at a wavelength of 627 nm, and 630-730 nm was used for detection.

Scanning electron microscopy (SEM):

SEM was performed on the gels using FEI SEM Apreo equipped with ETD detector. Both the collagenase treated gels and the non-treated gels were first fixed with 4% paraformaldehyde for 1 hour. This is followed by 3x rinsing in PBS for 10 minutes in each step of shaking. The gels were then rinsed twice with Milli-Q water for 15 minutes

each. The fixed gels were then subjected to a series of dehydration steps in ethanol and hexamethyldisilazane (HMDS) using the existing protocol [31]. Briefly, the gels were dehydrated first in ethanol dilution series: 30%, 50%, 70%, 90% and 100% for 15 minutes of each step. The gels were then incubated in ethanol/HMDS dilution series: 33%, 50%, 66% and 100% for 15 minutes each. After the final incubation, the gels were allowed to dry on an aluminum foil for at least 1 day in the fume hood. The dried gel samples were then sputter coated with a Pelco SC-7 sputter coater with gold as the target. The gels were then imaged at 5 kV and 0.6 nA with magnifications of 15000x and 30000x.

Lengths and diameters of fibrils:

The fibril lengths were measured using the fluorescence based on fast green staining. Images were obtained using confocal Leica SP8 imaging system. Fibril lengths were then analyzed using CT-FIRE v2.0 [32]. The parameters used are: Minimum fibril length, dangler length threshold (thresh dang L), short fibril length threshold (thresh short L), distance for linking sameoriented fibrils (thresh linkd), and minimum length of a free fibril (thresh flen), were all set to eight pixels. Default settings were used for all other fibril extraction parameters and output figure controls. We used MATLAB-based automated tool called SIMPoly (see [33] for details) which yields the collagen fibril diameters.

SI10 Single fibril model calibration and comparison:

We used the experimental data of Flynn et al. [18] on single fibril degradation to calibrate our single fibril model. Flynn et al. [18] reported the diameter of degrading single collagen fibril under different external loading condition in a 5 µM Clostridium histolyticum bacterial collagenase type A solution. To solve our single fibril model for the parameter sets reported in Flynn et al. [18], we need to obtain the number of enzymes N_e^0 for a fibril. Using their enzyme concentration, we estimated N_e^0 for a fibril in an approximate manner based on a volume element equivalent to the initial

volume of the fibril. For fibrils of initial diameter $d_f^0 = 415$ nm and $d_f^0 = 250$ nm, the values of N_e^0 are 2100 and 750, respectively, for a chosen length $\ell_f^0 = 4000$ nm. The value of $\tau_c = 1.4$ s is obtained by calibrating our model prediction to the single fibril data corresponding to $d_f^0 = 415$ nm under zero load condition (see Fig. 3a of the main text). The value of k_+^c used to calibrate our model is 0.583 s^{-1} (class I clostridium histolyticum collagenases and rat type I) [23]. In a nutshell, our single fibril model have satisfactorily captured the experimental findings of [18] (see Fig. 3a of the main text).

The choice of $\delta E_m = 0.013\, E_m$: The degradation rate reduces when the fibril is under external tension [34, 35, 18] (see Fig. 3a of the main text). Perhaps the external tension increases the stability of the triple helices in the fibril by increasing the energy barrier for enzymatic unwinding [36, 37, 38, 39, 40]. However, the cleavage mechanism can be different for the isolated tropocollagen (triple helix) molecules under external tension [41, 42]. For a fibril, the increase in the internal energy due to external loading can increase the energy barrier for enzymatic unwinding where the rate is proportional to $k_+^w \propto \exp\left(-2E_m/k_BT\right)$. The increase in the energy barrier results in the decrease in the rate of unwinding, implying a decrease in the rate of degradation.

It is difficult to provide a direct estimation of the increase in the energy barrier of enzymatic unwinding because of external loading. We have followed a simple analytical approach to obtain the increment in the energy following the work of Tonge et al. [38] and using a general expression for strain energy (purely elastic). Under external loading, we can write the increment in energy ΔU for a tropocollagen under low external load $f_{ext} = 2$ pN is

$$\Delta U \sim \frac{1}{2}\left(\frac{\pi}{4}\, d_{\mathrm{TC}}^2\left(\ell_{\mathrm{TC}} + \delta\ell\right)\right)\, \frac{f_{ext}}{(\pi/4)\, d_{\mathrm{TC}}^2}\, \frac{f_{ext}}{(\pi/4)\, d_{\mathrm{TC}}^2\, E_{\mathrm{TC}}}, \tag{S17}$$

where $\delta\ell$ is the extension and E_{TC} is the elastic modulus of a tropocollagen. The value of E_{TC} is in the range $0.01 - 1$ GPa [43, 44, 17]. For a chosen value $E_{\mathrm{TC}} \sim 0.5$ GPa and $\delta\ell$ in the range $50 - 250$ nm [44], (S17) yields to $\Delta U \sim 0.009\, E_m - 0.015\, E_m$, where

$E_m = n_{res}\,\Delta G/N_A$. Our model captured the experimental trend of Flynn et al. [18] well for $\delta E_m = 0.013\,E_m$.

The scaling related to single fibril degrdation: Figs. 3b,c of the main text imply that the degradability must be directly proportional to the number of enzymes per unit surface area of the fibril. According to the model assumptions, if the enzymes are not losing their activity and potency as enzymatic degradation progresses, then the surface area of the fibril is the only parameter which decreases with time. Thus a thicker fibril and a thinner fibril of same length can degrade up to a same extent if the ratio N_e^0/A_f^0, where $A_f^0 = (\pi d_f^0 \ell_f)$ is the area of the fibril, is fixed. This is reflected in Fig. S2a-c, where the same extent of degradation is observed if N_e^0/d_f^0 is a constant. The model predicts thicker fibrils with significantly larger number of enzymes to be highly degradable than thinner fibrils with very less number of enzymes subject to the ratio N_e^0/d_f^0, and *vice-versa*. The predictions are sensitive to the choice of k_+^c which varies with different MMPs and types of collagen. As expected, the extent of degradation decreases with the decrease in k_+^c.

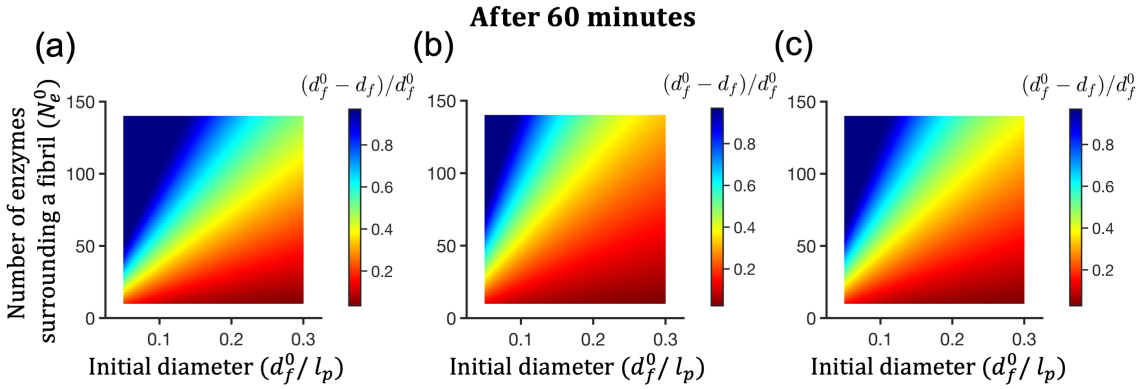

Figure S2: Degradation of single collagen fibril. (a)-(c) are color maps representing the extent of degradation after 1 hour for ranges of N_e^0 (number of enzymes surrounding a fibril) and d_f^0/l_p (initial fibril diameter) where $l_p = 1\,\mu$m is a nominal length scale. (a) fibril length $\ell_f/l_p = 2$, $k_+^c = 0.583$ s^{-1} [23]; (b) fibril length $\ell_f/l_p = 3$, $k_+^c = 0.583$ s^{-1}; (c) fibril length $\ell_f/l_p = 2$, $k_+^c = 0.472$ s^{-1} [21].

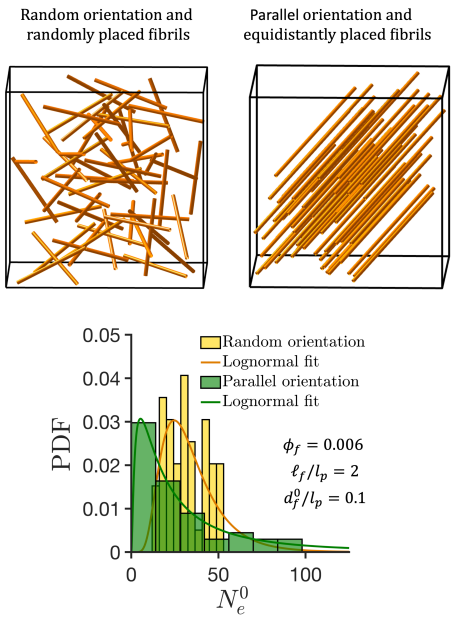

Figure S3: The enzyme distributions in two different configurations.

SI11 Model microstructure generation for P2 and P8 gels using the histograms of fibril diameters from the experiments:

We performed statistical comparisons by fitting log-normal distributions to individual images for both SEM and fast green stained images. We compared their mean and standard deviation values before and after degradation. We did not find significant differences in length distributions, but there are differences in the diameter distributions. Figure S4 shows the comparisons for the diameters.

The lognormal distribution curves fit our histrograms better than other distributions such as normal and gamma distributions (see Fig. S5).

We used the lognormal fitted curves of the diameter histograms (P2 and P8) from the experiments to generate the fibril distributions. The parameters related to the lognormal fits from P2 and P8 are $\mu_{P2} = -2.247$ and $\sigma_{P2} = 0.45$, and $\mu_{P8} = -2.288$ and $\sigma_{P8} = 0.4$, respectively. Using these values and lognormal function, random numbers

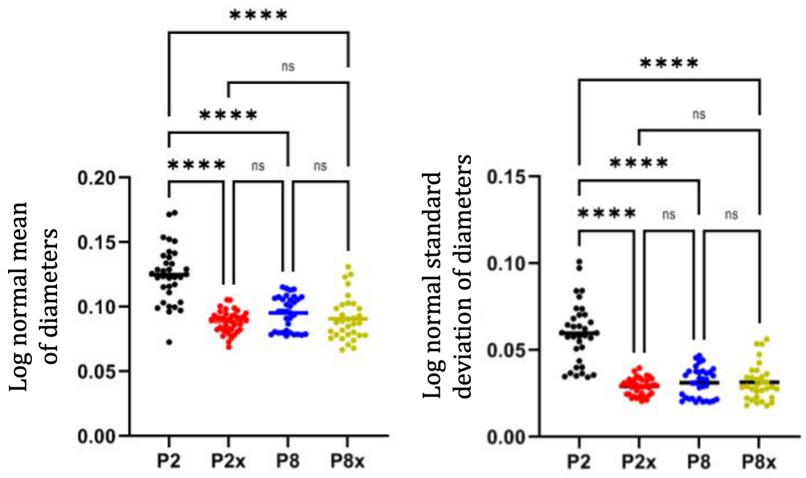

Figure S4: Comparisons of fibrils diameters from experiments. SEM images collected across three repeats were used for the analysis, N>33. Statistical significance was determined using one-way ANOVA, ****p <0.0001.

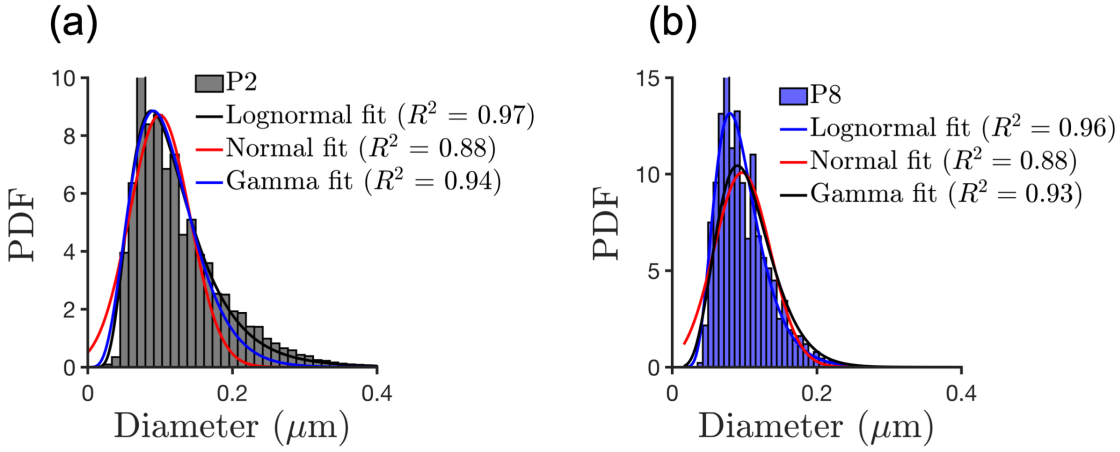

Figure S5: Different fits and goodness of fits for P2 (a) and P8 (b).

are generated in between 0.04-0.2 µm for P2, 0.03-0.16 µm for P8, and we ignore the tail regions where PDF is less than 2 (see Fig. S6a). In both P2 and P8, all fibrils are of same length. For P2, $\ell_f/l_p = 2$, and $\ell_f/l_p = 1.8$ for P8 which is 10% smaller than that of P2. We note in passing that in experiments, the mean length of P8 is found to be slightly (approx. 10 %) smaller than that of P2. For both P2 and P8, the distributions are generated such that the volume fraction of fibrils $\phi_f = 0.007$ turns out to be the same. The outcomes of number of fibrils n_f in P2 and P8 for simulation are 40 and 75, respectively. The chosen value of ϕ_f is close to the collagen concentration used in the experiments 2.5 mg/mL. For each P2 and P8, we performed three independent simulations, and we generated all three sets using the histograms of diameters from experiments (Fig. S6a). We showed the thickness distributions of the generated fibrils in Fig. S6b. The distributions generated for the simulations are qualitatively similar to those from the experiments.

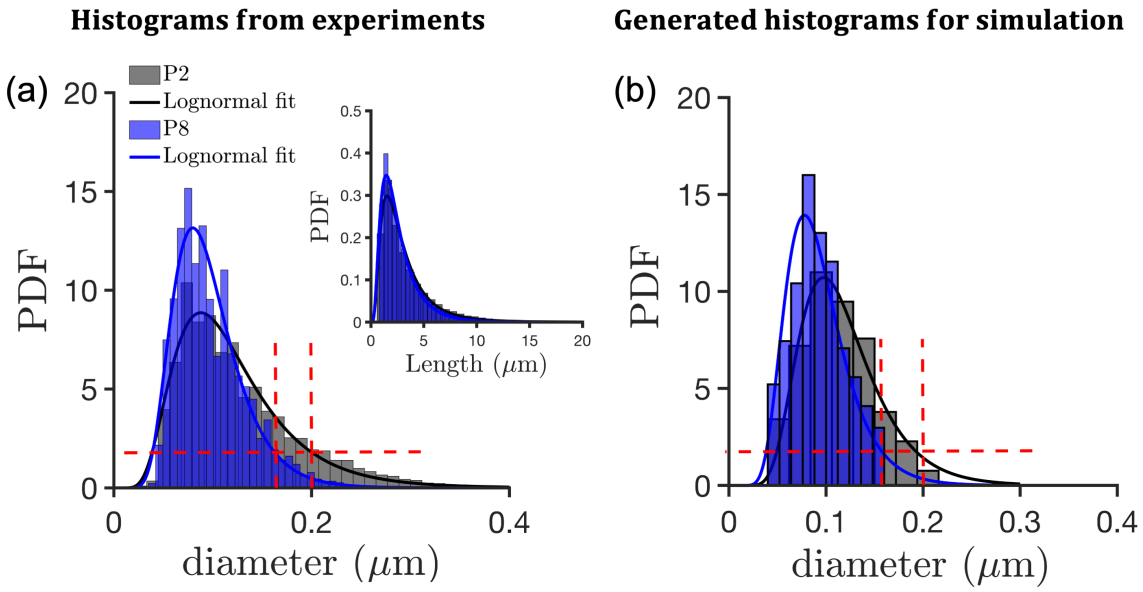

Figure S6: Histograms of diameters for P2 and P8 matrices. (a) From experiments. (b) Histograms are generated for hybrid simulation using (a).

References

[1] Adamczyk Z, Senger B, Voegel J, Schaaf P. Irreversible adsorption/deposition kinetics: A generalized approach. J Chem Phys. 1999;110:3118-28.

[2] Fang F, Satulovsky J, Szleifer I. Kinetics of protein adsorption and desorption on surfaces with grafted polymers. Biophys J. 2005;89:1516-33.

[3] Adamczyk Z. Kinetics of diffusion-controlled adsorption of colloid particles and proteins. JCIS. 2000;229:477-89.

[4] Schaaf P, Talbot J. Surface exclusion effects in adsorption processes. J Chem Phys. 1989;91:4401-9.

[5] Talbot J, Tarjus G, Van Tassel P, Viot P. From car parking to protein adsorption: an overview of sequential adsorption processes. Colloids and Surfaces A. 2000;165:287-324.

[6] Eckhard U, Schönauer E, Nüss D, Brandstetter H. Structure of collagenase G reveals a chew-and-digest mechanism of bacterial collagenolysis. Nat Struct Mol Biol. 2011;18:1109-14.

[7] Perumal S, Antipova O, Orgel J. Collagen fibril architecture, domain organization, and triple-helical conformation govern its proteolysis. Proc Nat Acad Sci. 2008;105:2824-9.

[8] Glasstone S, Laidler K, Eyring H. The theory of rate processes: the kinetics of chemical reactions, viscosity, diffusion and electrochemical phenomena. McGrawHill Book, New York. 1941.

[9] Stuart D, Anderson O. Dependence of ultimate strength of glass under constant load on temperature, ambient atmosphere, and time. J American Ceramic Soc. 1953;36:416-24.

[10] Adjari A, Brochard-Wyart F, de Gennes P, Leibler L, Viovy J, Rubinstein M. Slippage of an entangled polymer melt on a grafted surface. Physica A: Statistical Mechanics and its Applications. 1994;204:17-39.

[11] Sung W. Slippage of linear flows of entangled polymers on surfaces. Phys Rev E. 1995;51:5862.

[12] Vega D, Villar M, Alessandrini J, Valles E. Terminal relaxation of model poly (dimethylsiloxane) networks with pendant chains. Macromolecules. 2001;34:4591-6.

[13] Raphael E, De Gennes P. Rubber-rubber adhesion with connector molecules. J Phys Chem. 1992;96:4002-7.

[14] Léger L, Creton C. Adhesion mechanisms at soft polymer interfaces. Phil Tran Roy Soc A. 2008;366:1425-42.

[15] De Gennes P. Scaling concepts in polymer physics. Cornell university press; 1979.

[16] Shen Z, Kahn H, Ballarini R, Eppell S. Viscoelastic properties of isolated collagen fibrils. Biophys J. 2011;100:3008-15.

[17] Gautieri A, Vesentini S, Redaelli A, Buehler M. Viscoelastic properties of model segments of collagen molecules. Matrix Biology. 2012;31:141-9.

[18] Flynn B, Tilburey G, Ruberti J. Highly sensitive single-fibril erosion assay demonstrates mechanochemical switch in native collagen fibrils. BMMB. 2013;12:291-300.

[19] Ottl J, Gabriel D, Murphy G, Knäuper V, Tominaga Y, Nagase H, et al. Recognition and catabolism of synthetic heterotrimeric collagen peptides by matrix metalloproteinases. Chemistry & Biology. 2000;7:119-32.

[20] Saffarian S, Collier I, Marmer B, Elson E, Goldberg G. Interstitial collagenase is a Brownian ratchet driven by proteolysis of collagen. Science. 2004;306:108-11.

[21] Welgus H, Jeffrey J, Stricklin G, Eisen A. The gelatinolytic activity of human skin fibroblast collagenase. J Biol Chem. 1982;257:11534-9.

[22] Fields G, Van Wart H, Birkedal-Hansen H. Sequence specificity of human skin fibroblast collagenase. Evidence for the role of collagen structure in determining the collagenase cleavage site. J Biol Chem. 1987;262:6221-6.

[23] Mallya S, Mookhtiar K, Van Wart H. Kinetics of hydrolysis of type I, II, and III collagens by the class I and II Clostridium histolyticum collagenases. J Protein Chem. 1992;11:99-107.

[24] Lauer-Fields J, Tuzinski K, Shimokawa K, Nagase H, Fields G. Hydrolysis of triple-helical collagen peptide models by matrix metalloproteinases. J Biol Chem. 2000;275:13282-90.

[25] Salsas-Escat R, Nerenberg P, Stultz C. Cleavage site specificity and conformational selection in type I collagen degradation. Biochemistry. 2010;49:4147-58.

[26] Chung L, Dinakarpandian D, Yoshida N, Lauer-Fields J, Fields G, Visse R, et al. Collagenase unwinds triple-helical collagen prior to peptide bond hydrolysis. EMBO. 2004;23:3020-30.

[27] Tyn M, Gusek T. Prediction of diffusion coefficients of proteins. Biotech and Bioengg. 1990;35:327-38.

[28] Ranamukhaarachchi S, Modi R, Han A, Velez D, Kumar A, Engler A, et al. Macromolecular crowding tunes 3D collagen architecture and cell morphogenesis. Biomaterials Sci. 2019;7:618-33.

[29] León-López A, Morales-Peñaloza A, Martínez-Juárez V, Vargas-Torres A, Zeugolis D, Aguirre-Álvarez G. Hydrolyzed collagen—sources and applications. Molecules. 2019;24:4031.

[30] Tarnutzer K, Siva Sankar D, Dengjel J, Ewald C. Collagen constitutes about 12% in females and 17% in males of the total protein in mice. Sci Rep. 2023;13:4490.

[31] Raub C, Suresh V, Krasieva T, Lyubovitsky J, Mih J, Putnam A, et al. Noninvasive assessment of collagen gel microstructure and mechanics using multiphoton microscopy. Biophys J. 2007;92:2212-22.

[32] Bredfeldt J, Liu Y, Pehlke C, Conklin M, Szulczewski J, Inman D, et al. Computational segmentation of collagen fibers from second-harmonic generation images of breast cancer. J Biomedical Optics. 2014;19(1):016007-7.

[33] Murphy R, Turcott A, Banuelos L, Dowey E, Goodwin B, Cardinal K. Simpoly: A Matlab-based image analysis tool to measure electrospun polymer scaffold fiber diameter. Tissue Engineering Part C: Methods. 2020;26(12):628-36.

[34] Bhole A, Flynn B, Liles M, Saeidi N, Dimarzio C, Ruberti J. Mechanical strain enhances survivability of collagen micronetworks in the presence of collagenase: implications for load-bearing matrix growth and stability. Phil Tran Roy Soc A: Mathematical, Physical and Engineering Sciences. 2009;367:3339-62.

[35] Camp R, Liles M, Beale J, Saeidi N, Flynn B, Moore E, et al. Molecular mechanochemistry: low force switch slows enzymatic cleavage of human type I collagen monomer. J American Chem Soc. 2011;133:4073-8.

[36] Chang S, Flynn B, Ruberti J, Buehler M. Molecular mechanism of force induced stabilization of collagen against enzymatic breakdown. Biomaterials. 2012;33:3852-9.

[37] Chang S, Buehler M. Molecular biomechanics of collagen molecules. Materials Today. 2014;17:70-6.

[38] Tonge T, Ruberti J, Nguyen T. Micromechanical modeling study of mechanical inhibition of enzymatic degradation of collagen tissues. Biophysical J. 2015;109:2689-700.

[39] Saini K, Cho S, Dooling L, Discher D. Tension in fibrils suppresses their enzymatic degradation–A molecular mechanism for 'use it or lose it'. Matrix Biol. 2020;85:34-46.

[40] Topol H, Demirkoparan H, Pence T. Fibrillar collagen: A review of the mechanical modeling of strain-mediated enzymatic turnover. Applied Mech Rev. 2021;73:050802.

[41] Adhikari A, Chai J, Dunn A. Mechanical load induces a 100-fold increase in the rate of collagen proteolysis by MMP-1. J American Chem Soc. 2011;100:513a.

[42] Adhikari A, Glassey E, Dunn A. Conformational dynamics accompanying the proteolytic degradation of trimeric collagen I by collagenases. J American Chem Soc. 2012;134:13259-65.

[43] David L, Grood E, Noyes F, Zernicke R, et al. Biomechanics of ligaments and tendons. Exercise and sport sciences reviews. 1978;6:125-82.

[44] Sun Y, Luo Z, Fertala A, An K. Direct quantification of the flexibility of type I collagen monomer. Biochem Biophys Res Commun. 2002;295:382-6.